A PDES METHOD PRESERVING BOUNDARIES ON DENSE DISPARITY MAP RECONSTRUCTION

Ji liu[1,2], Junjian Peng[1,2], Yuechao Wang[2] and Yandong Tang[2]
[1]*Graduate University of Chinese Academy of Sciences, Beijing 100039, China*
[2]*Shenyang Institute of Automation, Chinese Academy of Sciences Shenyang 110016, China*

Keywords: Disparity map reconstruction, PDEs, GCPs.

Abstract: Over smoothness restricts the application of PDEs in the field of dense disparity map reconstruction, because disparity map reconstruction usually requires preserving discontinuousness in some areas such as the boundaries of objects. To preserve disparity discontinuousness, this paper adopts two strategies. Firstly, ground control points (GCPs) are introduced as the soft constraint. Secondly, this paper designs a structure of smoothness part in energy functional, which can preserve discontinuousness effectively. Moreover, the adjustable parameters in the smoothness part advance its robustness. In experiments, we compare proposed method with graph cuts method and prove that PDEs is also a useful solution for disparity map reconstruction and has the advantage of dealing with smooth images.

1 INTRODUCTION

Dense disparity map reconstruction based on two intensity images is the fundamental research in stereo vision. It can be described as matching each point in one image with its correspondent point in the other one. According to the epipolar constraint, all possible correspondent points lie in the same line. Thus, the matching relationship can be described as the disparity surface $D(x,y)$.

Over the years, numerous algorithms with energy functional optimization have been investigated in dense reconstruction via two or more images. In order to find the best disparity surface, many researches focus on functional optimization. Graph cuts and belief propagation, as two discrete functional optimization methods, have become two mainstream methods and won academic recognition (Marshall and William, 2003). In the field of disparity map reconstruction, the top contenders for the best disparity map estimation, on the most common comparison data, either use belief propagation (Sun et al., 2003) or graph cuts (Boykov et al., 2001). Many researches discuss the application of graph cuts (Roy and Cox, 1998; Birchfield and Tomasi, 1999; Kim et al., 2003) and belief propagation (Sun et al., 2003; Klaus et al., 2006; Frey et al., 2002; Felzenszwalb and Huttenlokcher, 2006) in disparity map reconstruction. Two papers (Kolmogorov and Zabih, 2004) and (Boykov, 2001) play the important role in the theory and application of graph cuts. In (Kolmogorov and Zabih, 2004), the author gives a precise characterization of what function can be minimized via graph cuts, and in (Boykov, 2001) the author introduces two efficient approximation algorithms to find a local minimum based on graph cuts. In paper (Sun et al., 2003; Frey et al., 2002; Felzenszwalb and Huttenlokcher, 2006), the authors propose some fast and effective approximation algorithms for belief propagation. Overall, two methods have been studied broadly and can be considered as comparatively mature algorithms in disparity map reconstruction. This paper harvests considerable profits from their works.

PDEs mothed, as a continuous functional optimization method, has been applied successfully in image segmentation (Aubert et al., 2002; Maso et al., 1992; Kass et al., 1988), 3D reconstruction (Faugeras and Keriven, 1998; Deriche et al., 1997; Faugeras and Keriven, 2002), and image recovery (Aubert and Vese, 1997). However, compared with graph cuts and belief propagation, PDEs has not been applied broadly in the disparity map reconstruction. The PDEs method always assumes that images can be approximately considered as continuous functions. Regrettably, the assumption often can not be satisfied in the disparity map reconstruction, since the ultimate disparity map result needs to preserve discontinuousness in some disparity mutation areas such as the object's

liu J., Peng J., Wang Y. and Tang Y. (2008).
A PDES METHOD PRESERVING BOUNDARIES ON DENSE DISPARITY MAP RECONSTRUCTION.
In *Proceedings of the Third International Conference on Computer Vision Theory and Applications*, pages 655-661
DOI: 10.5220/0001080606550661

boundaries. Thus, PDEs method performs very well in those fields where images are fit to be considered as continuous function but is not very effective in disparity map reconstruction. This reason leads to fewer researches on PDEs application in this field than graph cuts and belief propagation.

Since PDEs method has its advantage in dealing continuous situation, this paper still adopts this method to estimate the disparity map. We hope to benefit from its advantage and avoid its drawback. Although we assume that images are continuous functions, the disparity map calculated via images can still generate discontinuousness to meet the expected disparity map. Robert and Deriche (Robert and Deriche, 1996), in order to preserve discontinuous boundaries, design the smoothness function to satisfy that all points should diffuse mainly in the orthogonal direction of disparity gradient. Alvarez L. et al. (Alvarez et al., 2000) use the smoothness function introduced by Nagel and Engelmann which constrains the diffuse direction mainly in the colour gradient direction. Their works are to some extent effective to preserve discontinuousness and enlighten us a lot.

In order to preserve discontinuities better, this paper adopts two strategies: ground control points (GCPs) are applied as the soft constraint conditions and the image gradient information is introduced to control the penalty strength in the smoothness function.

For the former, the ground control points (GCPs) have two features. Firstly, they usually appear in the areas where the colour changes suddenly, for example, the boundaries of objects. Secondly, the disparity value in GCPs can be gained by some simple local matching algorithms such as SSD, ZNCC, and have high reliability. So, proposed method utilizes the prior information of GCPs to modify the common cost part of the energy function.

For the latter, the smoothness function serves to smoothness the disparity surface by penalizing the variation between neighbour points. However, some variation should be preserved or not be penalized if the variation appears on the object boundaries. The image gradient information is used to distinguish boundaries or non-boundaries. Thus, we introduce the image gradient information to control the penalty strength. To satisfy different images, we design a general mathematical model for the smoothness function, which contains several adjustable parameters for different images.

Finally, according to variational principles, the Euler-Lagrange equations are deduced. Through iteratively numerical solving Euler-Lagrange equations, the disparity map solutions can be calculated. For lessening the probability of local minimum, the scale-space approach is utilized as (Alvarez et al., 2000; Alvarez et al., 1999).

The paper is organized as follows: In Section 2, we describe how to detect the GCPs. In Section 3, the energy functional is introduced. The common cost function will be modified based on the information of GCPs. We analyze the conditions that should be satisfied by the smoothness function and propose a general mathematical model for the smoothness function. In Section 4, the numerical schemes of Euler-Lagrange equation and the scale-space approach are represented. In Section 5, the experimental results are presented to validate the GCPs method. This paper ends with a brief discussion and conclusion in section 6.

2 GCPS

GCPs can provide some more reliable information for matching. For preserving the boundary discontinuousness, we want to find out some GCPs at the Image's boundaries. This method may be a little similar as the method in (Kim et al., 2002). Firstly, all the images are processed by the LOG filter to generate the new images. Secondly, the new images are filtered by a defined filter with N directions as figure 1, which are depicted in (1).

$$f_\theta(x,y)=\begin{cases}1-\left|x\sin\theta-y\cos\theta\right| & if\ \left|x\sin\theta-y\cos\theta\right|<1\\ 0 & otherwise\end{cases} \quad (1)$$

To avoid the problem that filters are across the object boundaries, we perform local matching using three filters for each orientation, where the centers of the filters are shifted to the three different positions as figure 2, and only the best filtering result (the minimum) is preserved. Thus, each pixel contains N results. All pixels are classified into two groups (homogeneous group and heterogeneous group). If the maximum of the pixel's N results exceeds a certain threshold, this pixel is labeled as heterogeneous pixel; otherwise, it is labeled as homogeneous pixel. All the GCPs will come from the heterogeneous pixels. Thirdly, only those pixels which satisfy the constraint of consistent bi-directional matching can became GCPs. It is operated as follows: in the disparity range, each heterogeneous pixel in the left image is matched with the pixel in the right image according to ZNCC measurement. Then, if the best matching pixel in the right image is a heterogeneous pixel and its best matching pixel in the left image is consistent, this pixel can be defined as the GCP and its disparity value will be recorded.

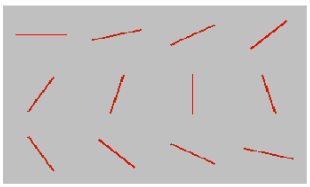

Figure 1: Examples of the rod-shaped oriented filters in interval of 15°.

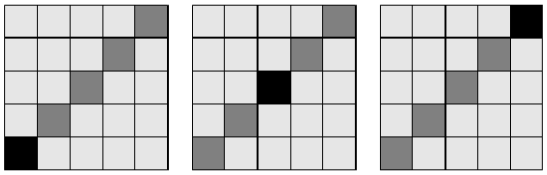

Figure 2: Diagram of the three shiftable oriented filters, where the centers of the filters are marked in black.

3 THE ENERGY FUNCTIONAL

Generally, the energy function contains two parts in (2)

$$E(D)=\iint_{\Omega} C(D(x,y),x,y)+\lambda S(\nabla D(x,y))dxdy \qquad (2)$$

where the $C(\bullet)$ is the cost function, the $S(\bullet)$ is the smoothness function and Ω is the image domain.

3.1 The Cost Function

According to the assumption of Lambertian surfaces, i.e. of objects that look equally bright from all viewing directions, the two points accurately matched have the similar intensity in general. Thus, we define the cost function as follows:

$$C(D,i,j)=\left(I_1(i,j)-I_2(i,j-D(i,j))\right)^2 \qquad (3)$$

where I_n is the intensity in image n =1,2. We assume two images have been rectified so that the disparity only appears on the y axis. Equation (3) is the common frame of the cost part.

However, the expression of equation (3) is inclined to lead to local minimum. Because it is high possible that the grey value of one point in left image I_1 is equal to the grey value of more than one points in I_2. Several disparity values of a point may make the cost part equal to zero. When a certain wrong value of disparity in one point cause the cost part is zero, the result may be a local minimum.

In order to reduce the possibility of the local minimum, we utilize the prior knowledge of GCPs to flexibly limit the cost function. If a point has been established as GCPs, the real disparity at this point should be close to the disparity value $\overline{D}_{i,j}$ calculated during finding out GCPs. The longer the distance between them is, the larger the cost value is. Thus, we can design the cost function as (4). The frame can ensure that only one minimum in GCPs. Thus, to some extent, the frame can reduce the possibility of local minimum.

$$\overline{C}(D(i,j),i,j)=\begin{cases}\dfrac{a\left(\dfrac{D(i,j)-\overline{D}_{i,j}}{b}\right)^2}{1+\left(\dfrac{D(i,j)-\overline{D}_{i,j}}{b}\right)^2} & (i,j)\in GCPs\\ (I_1(i,j)-I_1(i,j-D(i,j)))^2 & otherwise\end{cases} \qquad (4)$$

3.2 The Smoothness Function

The smoothness function is necessary so as to smooth the disparity surface, since it can be used to limit the excessive coarseness of the disparity surface or the discontinuities of $D(x,y)$. So, it should be penalized if too large, and the larger the variation value is, the more the penalty is. However, the variation at different points should not be penalized as the same rules. For example, the variation appearing at the boundary is rational because we expect it to be discontinuous there, while the variation appearing at non-boundaries should be penalized severely. Thus, we utilized the image information to control the penalty strength and emphasis.

$\nabla D(x,y)$ represents the smoothness feature of disparity surface. The penalty about $\nabla D(x,y)$ contains two terms: the penalty about $|\nabla D|$ and the penalty about $\frac{|\nabla D\bullet\nabla I^{\perp}|}{|\nabla I|}$. The former means the disparity surface is required to be as smooth as possible. $\frac{|\nabla D\bullet\nabla I^{\perp}|}{|\nabla I|}$ presents the projection of the gradient disparity in the direction of the image gradient. So the penalty about it means that the gradient direction of disparity is supposed to be consistent with the image gradient direction. If a point locates in the non-boundary, we more emphasize the penalty about $|\nabla D|$ in this point than its disparity gradient direction. If a point locates in the boundary, the penalty about $\frac{|\nabla D\bullet\nabla I^{\perp}|}{|\nabla I|}$ is more important. The penalty emphasis and strength in a

point (*x*, *y*) depends on whether the point is at the boundary or not. For convenience, we utilize the image gradient information to sign whether the point is at the boundary (actually, there is other image information which can be used to sign the boundary, and we will discuss them in our future work). Usually, the boundary is linked with image gradient module.

Summarily, the smoothness function is described as this model:

$$S(\nabla D, \nabla I) = \alpha(|\nabla I|)S_1(|\nabla D|) + \beta(|\nabla I|)S_2(\frac{|\nabla D \bullet \nabla I^{\perp}|}{|\nabla I|}) \quad (5)$$

where $S_1(|\nabla D|)$ presents the function of $|\nabla D|$, such as $S_1(|\nabla D|) = |\nabla D|^2$; $S_2(\frac{|\nabla D \bullet \nabla I^{\perp}|}{|\nabla I|})$ is similar to $S_1(|\nabla D|)$; $\alpha(|\nabla I|)$ presents the weight of the penalty of $S_1(|\nabla D|)$ and $\beta(|\nabla I|)$ presents the weight of the penalty of $S_2(\frac{|\nabla D \bullet \nabla I^{\perp}|}{|\nabla I|})$.

Estimating $\alpha(|\nabla I|)$ and $\beta(|\nabla I|)$ is the key of estimating the smoothness function. We depict the constraint conditions of $\alpha(|\nabla I|)$ and $\beta(|\nabla I|)$ as below. Firstly, $\alpha(|\nabla I|)$ and $\beta(|\nabla I|)$ must be regularized:

$$\alpha(|\nabla I|) + \beta(|\nabla I|) = 1 \quad (6)$$

$$a > 0 \quad \beta > 0 \quad (7)$$

The larger $|\nabla D|$ at a point is, the more probably it is at the boundary. The opposite is similar. Thus, we can get:

$$\begin{cases} a(|\nabla I|) > \beta(|\nabla I|) & if \quad |\nabla I| < b \\ a(|\nabla I|) < \beta(|\nabla I|) & if \quad |\nabla I| > b \end{cases} \quad (8)$$

where *b* is considered as the threshold to estimate whether the point (*x*, *y*) is at the boundary or not. Naturally, we can assume

$$\begin{cases} \frac{\partial \alpha}{\partial |\nabla I|} < 0 \\ \frac{\partial \beta}{\partial |\nabla I|} > 0 \end{cases} \quad (9)$$

In addition, for decreasing the ambiguousness near the threshold, we require that the weight $\alpha(|\nabla I|)$ rapidly descends at a gradually fast speed while $|\nabla I|$ approaches the threshold from left, and the descending speed begins to lower while $|\nabla I|$ leaves the threshold from right. Thus, we add additional conditions about α and β :

$$\begin{cases} \frac{\partial^2 \alpha}{\partial |\nabla I|^2} < 0, \frac{\partial^2 \beta}{\partial |\nabla I|^2} > 0 & if \quad |\nabla I| < b \\ \frac{\partial^2 \alpha}{\partial |\nabla I|^2} > 0, \frac{\partial^2 \beta}{\partial |\nabla I|^2} < 0 & if \quad |\nabla I| > b \end{cases} \quad (10)$$

Based on all conditions above, $\alpha(|\nabla I|)$ and $\beta(|\nabla I|)$ can be approximately figured as figure 3, where $r_0 = \lim_{|\nabla I| \to 0} \beta(|\nabla I|)$ and $r_t = \lim_{|\nabla I| \to \infty} \beta(|\nabla I|)$

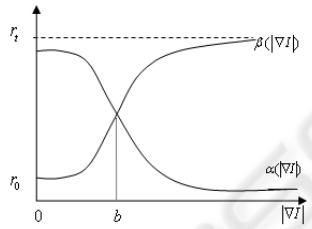

Figure 3: Sketchy map of $\alpha(|\nabla I|)$ and $\beta(|\nabla I|)$.

Then, we define the model of $\beta(|\nabla I|)$ as (11) and $\alpha(|\nabla I|)$ can be calculated through $\alpha(|\nabla I|) = 1 - \beta(|\nabla I|)$ according to (6).

$$\beta(|\nabla I|) = \frac{e|\nabla I|^m + f}{|\nabla I|^m + g} \quad (11)$$

where *e*, *f*, *g*, and m are constants. According to conditions (6)-(9), these results are in (12).

$$\begin{cases} e = r_t \\ g = \frac{2r_t - 1}{1 - 2r_0} b^m \quad \text{and} \quad m > 0, 0 < r_0 < r_t < 1 \\ f = \frac{2r_t - 1}{1 - 2r_0} b^m r_0 \end{cases} \quad (12)$$

where *m* is decided by the additional conditions (10).

$$m = \frac{r_t - r_0}{r_t + r_0 - 1} \text{ and } r_t + r_0 > 1 \quad (13)$$

4 SOLVING EULER-LAGRANGE EQUATIONS

According to the variational principles, *D*(*x*, *y*) as the minimum of (1) must fulfill the Euler-Lagrange equations and boundary conditions:

$$\begin{cases} C_D - \lambda(\frac{\partial}{\partial x} S_{D_x} + \frac{\partial}{\partial y} S_{D_y}) = 0 \\ \frac{\partial S}{\partial D_x} \cos \nu + \frac{\partial S}{\partial D_y} \sin \nu = 0 \end{cases} \quad (14)$$

where $\begin{bmatrix}\cos\nu\\ \sin\nu\end{bmatrix}$ represents a vector normal to the boundary of Ω. Equation (14) is solved by the gradient-descent method or, equivalently, by using a dynamic scheme as (15)

$$\begin{cases}\dfrac{\partial D(t,x,y)}{\partial t} = -C_D + \lambda\left(\dfrac{\partial}{\partial x}S_{D_x} + \dfrac{\partial}{\partial y}S_{D_y}\right)\\ \dfrac{\partial S}{\partial D_x}\cos\nu + \dfrac{\partial S}{\partial D_y}\sin\nu = 0\end{cases} \tag{15}$$

where t is an artificial time.

We discretize the equation by finite differences. All spatial derivatives are approximated by central differences, and for the discretization in t we use explicit scheme as (16).

$$\begin{aligned}&\frac{D(t+\Delta t,i,j)-D(t,i,j)}{\Delta t} = -C_D(D(t,i,j),i,j)\\ &+\lambda\left(\frac{\partial S_{D_x}}{\partial x}(D(t,i,j)) + \frac{\partial S_{D_y}}{\partial y}(D(t,i,j))\right)\end{aligned} \tag{16}$$

To avoid the local minimum, a linear scale-space approach is applied. Typically, we may expect that the algorithm converges to a local minimum of the energy functional that is located in the vicinity of the initial data. To avoid convergence to irrelevant local minimum, we embed proposed method into a linear scale-space framework (Robert and Deriche, 2000). We let $I_1^\sigma := G_\sigma * I_1$ and $I_2^\sigma := G_\sigma * I_2$, where * is the convolution operator, and G_σ detects a Gaussian with standard deviation σ. We start with a large initial scale σ_0. Then we compute the disparity D_{σ_0} at scale σ_0 as the asymptotic state of solution using some initial approximation. Next, we choose a number of scales: $\sigma_n = \eta\sigma_{n-1}, \eta \in (0,1)$, and we get the D_{σ_i} at each σ_i with the initial of $D_{\sigma_{i-1}}$. Overall, we can modify the iterating formation as:

$$\begin{aligned}&\frac{D^{\sigma_i}(t+\Delta t,i,j)-D^{\sigma_i}(t,i,j)}{\Delta t} = -\overline{C}^{\sigma_i}{}_D(D^{\sigma_i}(t,i,j),x,y)\\ &+\lambda\left(\frac{\partial S_{D_x}}{\partial x}(D^{\sigma_i}(t,i,j)) + \frac{\partial S_{D_y}}{\partial y}(D^{\sigma_i}(t,i,j))\right)\\ &\overline{C}^{\sigma_i}(D(i,j),i,j) = \begin{cases}\dfrac{k\left(\frac{D^{\sigma_i}(i,j)-\overline{D}_{i,j}}{g}\right)^2}{1+\left(\frac{D^{\sigma_i}(i,j)-\overline{D}_{i,j}}{g}\right)^2} & (i,j)\in GCPs\\ (I_1^{\sigma_i}(i,j)-I_2^{\sigma_i}(i,j-D^{\sigma_i}(i,j)))^2 & otherwise\end{cases}\\ &D^{\sigma_{i+1}}(0,i,j) = D^{\sigma_i}(\infty,i,j)\end{aligned} \tag{17}$$

5 RESULTS

In this section, we compare proposed method without considering occlusion with graph cuts method. All the experiment images come from the website http://vision.middlebury.edu/stereo. The images "cloth1" and "cloth3" are contained in the 2006 datasets, the image "Teddy" is in the 2003 database and the image "Tsukuba" is in the 2001 database. In order to evaluate proposed method, the recognized evaluations (Scharstein and Szeliski, 2001) are defined as (18) and (19).

$$R = \left(\frac{1}{N}\sum_{(x,y)}\left|disparityMap(x,y) - groundTruth(x,y)\right|^2\right)^{\frac{1}{2}} \tag{18}$$

$$B = \frac{1}{N}\sum_{(x,y)}\left(\left|disparityMap(x,y) - groundTruth(x,y)\right| > \Delta\right) \tag{19}$$

where N is the total number of pixels, Δ is a disparity error tolerance. For the experiments in the paper we use $\Delta = 1$. R denotes the average error value and B denotes the ratio of the "bad pixels" in the disparity map. The consequences are showed in table 1 and figure 4. In the results of proposed method, the boundaries of objects can be distinguished clearly. It indicates that the proposed method owns to the ability of preserving discontinuousness.

Table 1 presents that the average error value R in proposed method is lower than graph cuts method. It is mainly because that PDEs method has the characteristic of keeping continuousness. We list the detail comparison in figure 5. In some continuous areas, the proposed method can keep the disparity map continuous better than graph cuts method. The proportion of "bad pixels" in our method has no advantage comparing with graph cuts methods, especially in the image "Tsukuba" with much discontinuousness. The comparison in "Tsukuba" of table 1 can reflect this point.

Table 1: Error comparison. The code of GC method comes from the same website above.

	Cloth1 R/B	Cloth3 R/B	Tsukuba R/B	Teddy R/B
GC method	1.015 0.0104	1.766 0.0414	1.247 0.0424	4.9603 0.1317
Proposed method	0.604 0.0092	0.889 0.0247	0.809 0.0858	1.7703 0.1681

6 CONCLUSIONS

The assumption of continuousness renders PDEs method difficult to perfectly reconstruct disparity map. This paper adopts two strategies to preserve necessary discontinuousness for the disparity map. The results show that proposed method performs better than graph cuts method in "Cloth1" and "Cloth3", mainly because there images with less discontinuousness meet the feature of PDEs. The proposed method can deal with images with much

discontinuousness such as “Tsukuba” and “Teddy” and gain approximate results of graph cuts method.

There are some other aspects which can be improved. For example, occlusion problem should be considered, and this problem has exposed in “Tsukuba” and “Teddy”.

Although it is more difficult for the PDEs method to preserves boundaries than some discrete energy methods such as graph cuts method, PDEs methods have its advantage on keep continuousness. If we can find some witty strategies to preserve necessary discontinuousness, PDEs method still can become a useful solution in disparity map reconstruction.

REFERENCES

Alvarez, L., Deriche, R., Sanchez, J., Weickert, J., 2000. Dense disparity map estimation respecting image discontinuities: a PDE and scale-space based approach. In *Technical Report RR-3874, INRIA.*

Alvarez, L., Weickert, J., Sanchez, J., 1999. A scale-space approach to nonlocal optical flow calculations. In *Scale-Space Theories in Computer Vision*, pages 235-246.

Aubert, G., Barlaud, M., Faugeras, O. and Jehan-Besson, S., 2002. Image segmentation using active contours: Calculus of variations or shape gradients? In *Research Report, INRIA.*

Aubert, G., Vese, L., 1997. A variational method in image recovery. In *SIAM Journal of Numerical Analysis*, volume 34, pages 1948–1979.

Birchfield, S., Tomasi, C., 1999. Multiway cut for stereo and motion with slanted surfaces, *Proceeding of International Conference Computer Vision*, pages 489-495.

Boykov, Y., Veksler, O., Zabih R., 2001. Fast approximate Energy Minimization via Graph Cuts. In *Proceeding IEEE Transaction Pattern Analysis and Machine Intelligence*, volume 23**,** pages 1222-1239.

Chan, T. F., Vese, L.A., 2001. Active contours without edges. In *IEEE Transaction on Image Processing*, volume 10, pages 366-277.

Deriche, R., Bouvin, S., Faugeras, O., 1997. A level-set approach for stereo. In *Proceeding SPIE, Investigative Image Processing*, volume 2092, pages 150-161.

Faugeras, O., Keriven, R., 1998. Complete Dense Stereo vision Using Level Set Methods. In *Proceeding European Conference on Computer Vision*, pages 379-394.

Faugeras, O., Keriven, R., 2002. Variational Principles, Surface Evolution, PDE's, Level Set Methods and the Stereo Problem. In *IEEE Transaction on Image Processing*, volume **7,** pages 336-344.

Felzenszwalb, P. F., Huttenlokcher, D. P., 2004. Efficient Belief Propagation for Early Vision. In *Proceeding International Journal of Computer Vision*, volume 1, pages 261-268.

Frey B. J., Koetter R., Petrovic N., 2002. Very loopy belief propagation for unwrapping phase images. In *MIT Press*, volume 14.

Kass, M., Witkin, A., Terzopoulos D., 1988. Snakes: active contour models. In *International Journal of Computer Visiosn*, volume 1, pages 321–331.

Kim, J.C., Lee, K.M., Choi, B.T., Lee, S.U., 2005. A dense stereo matching using two-pass dynamic programming with generalized ground control points. *Proceeding Computer Vision and Pattern Recognition*, pages 1075-1082

Kim, J., Kolmogorov, V., Zabih, R., 2003. Visual correspondence using energy minimization and mutual information. In *Proceeding International Conference Computer Vision*, pages 1033-1040.

Klaus, A., Sormann, M., Karner, K, 2006. Segment-based stereo matching using belief propagation and a self-adapting dissimilarity measure, In *International Conference of Pattern and Recognition*, volume 3, pages 15-18.

Kolmogorov, V., Zabih, R., 2004. What energy functions can be minimized via graph cuts? In *IEEE Trans. Pattern Analysis and Machine Intelligence*, volume 28, pages 147-159.

Marshall, F. T., William, T. F., 2003. Comparison of Graph Cuts with Belief Propagation for Stereo, using Identical MRF Parameters. In *Proceedings of the Ninth IEEE International Conference on Computer Vision*, volume 2, pages 900-906.

Maso, G. D., Morel, J. M., Solimini, S., 1992. A variational method in image segmentation: existence and approximation results, In *Acta Matematica*, volume 168, pages 89–151.

Osher, S., Sethian, J.A., 1988. Fronts propagating with curvature dependent. In *Journal of Computational Physics*, volume 79, pages 12-49.

Robert, L., Deriche, R., 1996. Dense disparity map reconstruction: A minimization and regularization approach which preserves discontinuities. In *Proceeding European Conference on Computer Vision*, pages 439-451.

Roy, S., Cox, I., 1998. A maximum-flow formulation of the n-camera stereo correspondence problem. In *Proceeding international Conference of Computer Vision*, pages 492-498.

Scharstein, D., Szeliski, R., 2002. A taxonomy and evaluation of dense two-frame stereo orrespond- dence algorithms, In *International Journal of Computer Vision*, volume 47, pages 7-42.

Sun, J., Zheng, N.N., Shum, H.Y., 2003. Stereo Matching Using Belief Propagation. In *IEEE Trans. Pattern Analysis and Machine Intelligence*, volume 25, pages 787-800.

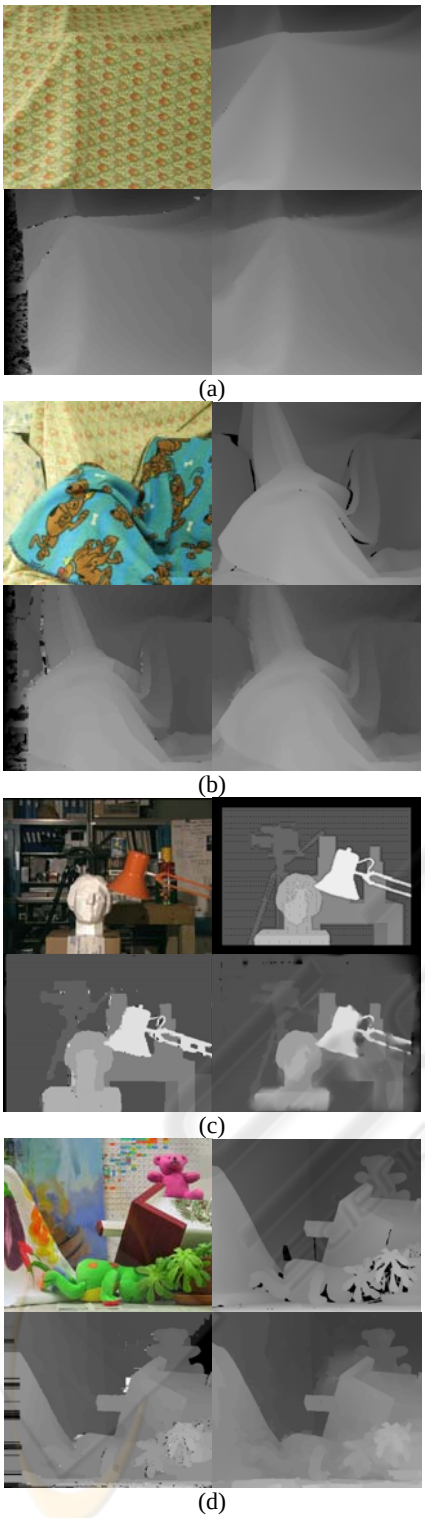

(a) (b) (c) (d)

Figure 4: The disparity map reconstructed by proposed method and graph cuts. Four group images (a) (b) (c) (d) respectively are related to Cloth1, Cloth3, Tsukuba and Teddy. In each group, the left-up, right-up, left-down and right-down images are respectively left image, ground truth, the result of GC and the result of proposed method.

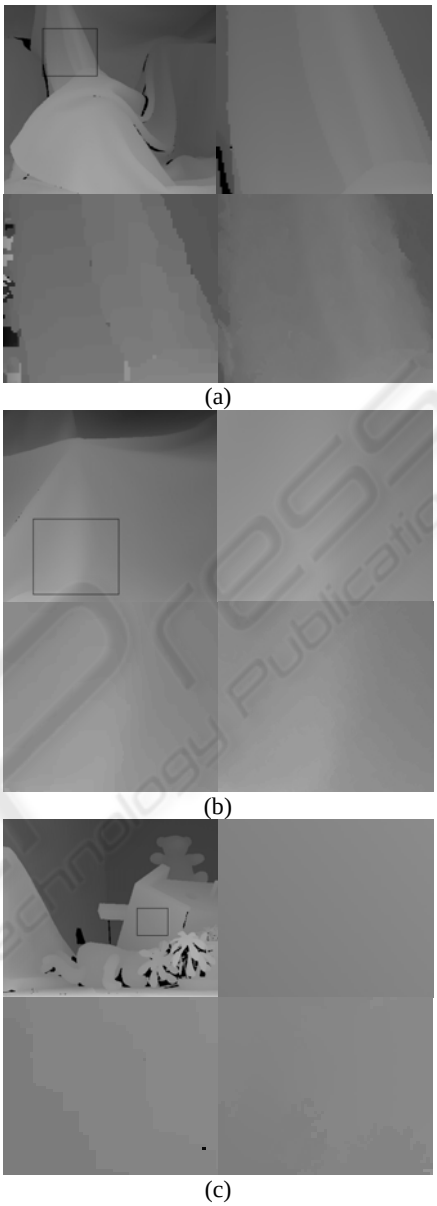

(a) (b) (c)

Figure 5: The detail comparison of disparity maps. Three group images (a) (b) (c) respectively are related to Cloth3, Cloth1 and Teddy. In each group, the left-up, right-up, left-down and right-down images are respectively ground truth, local ground truth, local result of GC and local result of proposed method.